A spark plasma sintering densification modeling approach: from polymer, metals to ceramics

Charles Manière, Lise Durand, Geoffroy Chevallier, Claude Estournès

A spark plasma sintering densification modeling approach: from polymer, metals to ceramics

Charles Manière[1,2], Lise Durand[2], Geoffroy Chevallier[1], and Claude Estournès[1,*]

[1] Université de Toulouse, CIRIMAT, CNRS INPT UPS, Université Paul-Sabatier, 118 route de Narbonne, 31062 Toulouse Cedex 9, France
[2] CEMES, CNRS UPR 8011, Université de Toulouse, 29 rue Jeanne Marvig, 31055 Toulouse, France

ABSTRACT

The powder compaction modeling of advanced sintering techniques such as spark plasma sintering is a crucial step in the conception of complex shape objects and the understanding of the process. The complete identification of common powder compaction models requires lengthy experimental investigations based on creep and compaction tests. In order to circumvent this problem, a semi-theoretical approach can be employed whereby the mechanical behavior of the powder material is determined theoretically and the temperature-dependent equivalent creep behavior of the material is determined experimentally. Extending the use of this approach to polymers, metals and ceramics is discussed and compared to other independent methods.

Introduction

The modeling of the powder compaction in spark plasma sintering is a key step in the engineering of complex shapes. Establishing all the constitutive parameters required for a sintering model constitutes a challenge that classically entails extensive experimental studies. A comprehensive sintering model should take into account:

- The dense material deformation behavior (often associated with linear viscous or creep power law),
- the mechanical moduli (describing the deformation behavior of the porous medium),
- the sintering stress,
- and possible specific parameters that may vary depending on the sintering techniques [1–3]. Parameters such as the current, the electromagnetic field, the local stress, local temperature gradients or the presence of plasma may accelerate the sintering kinetics [4–6].

Aside from the last-cited parameters that need to be identified by comparison with the pure thermomechanical behavior, the main challenge with the determination of classical sintering models lies in the experimental deconvolution of the temperature-dependent creep behavior (that describe the dense phase behavior) and the porosity-dependent moduli (governing the porous material behavior). In the case of spark plasma sintering, at least four model

Address correspondence to E-mail: estournes@chimie.ups-tlse.fr

parameters (creep and moduli parameters) are required, but the experiments only provide two information, the displacement and the applied load. The classical approach employed to establish a compaction model consists in performing experiments in different loading modes (die compaction, sinter-forging, isostatic loading, forging etc.). Classically, the power law creep is determined at different temperatures by creep tests on full dense samples. The porosity-dependent moduli are determined by hot isostatic pressing and sinter-forging tests on samples at different porosity rates [7]. A simpler approach based on die compaction and sinter-forging has been adapted to spark plasma sintering (SPS) for Ti–6Al–4V [8] and TiAl [9] and Ni [10]. These approaches facilitate the identification of all the sintering parameters, but they require extensive testing in order to reach the deconvolution of all the compulsory parameters. It is also to be noted that full dense creep tests for the identification of the power law creep may yield a different behavior if the specimen is subjected to phase transition, particularly during the densification stage or to grain growth that is particularly significant in high density ceramics. Setting aside stable large grain size alloys (less sensible to grain growth), the classical method does not easily apply to ceramics or nano-sized metals. To address this problem, in situ methods may be preferable. In this paper, a direct in situ method is considered based on a previously described method [11] and applied to various materials. Using this approach, the porosity-dependent moduli are determined by means of a theoretical law and the creep parameters are identified via simple SPS tests. A comparison of the stress exponents n obtained via the in situ approach and by the method of Li et al. [12] will be made. The in situ approach will also be analyzed using the Skorohod [13] and Abouaf [7, 8] models for Ti–6Al–4V. Finally, the accuracy of the in situ methods in regard to the basic material classes (polymer, metal and alloy, ceramic) will be discussed.

In situ methods of sintering parameters extraction

Regression approach for the identification of the creep parameters

The in situ methods based on the continuum theory of sintering [2] consider the following hypothesis:

1. the generalized porosity-dependent moduli determined by Skorohod [13] provides a reasonable approximation of the stress/strain distribution in the equivalent porous medium represented by the powder
2. the material ductility potentially influenced by the heating rate and the electric current can be described by a general exponential form of temperature dependence [14, 15]
3. the temperature/pressure gradients in the sample are negligible (reasonable in small sample sizes)
4. the powder/die friction is low. It has been experimentally demonstrated that for small pellet geometry and the use of a lateral graphite foil, the powder/die friction is very low [16].

Based on the above hypothesis, we have realized it is possible to identify the creep parameters employing Skorohod moduli [13]. Based on hypothesis number 2, a constant heating rate regime regression can be analyzed assuming an Arrhenius-type ductile behavior. This behavior can predict the evolution of ductility that increases and accelerates with the temperature. As we have already shown in ref. [11], the regression equation for this method is the following:

$$n \ln\left(\frac{|\sigma_z|}{\left(\psi+\frac{2}{3}\varphi\right)^{\frac{n+1}{2n}}(1-\theta)^{\frac{n-1}{2n}}|\dot{\varepsilon}_z|^{\frac{1}{n}}}\right) - \ln(T) = -\ln(A_0) + \frac{Q}{RT} \quad (1)$$

where n is the dimensionless power law creep stress exponent, $|\sigma_z|$ the applied stress (Pa), $|\dot{\varepsilon}_z|$ the specimen strain rate (s^{-1}), θ the porosity rate, T the temperature (K), R the gas constant (J K^{-1} mol^{-1}), φ and ψ are the dimensionless shear and bulk moduli determined here by Skorohod [13], A_0 and Q the pre-exponential constant (K s^{-1} Pa^{-n}) and activation energy (J mol^{-1}) of the power law creep Arrhenius term.

In this method, the parameters A_0 and Q are determined for different values of n. In the original method [11], the n value is determined by comparison of the curves shape for each n values (*between* 1 *and* 5 *here*). As it will be discussed later, this qualitative identification of n is not always possible due to the accuracy of the comparison of the curves at different n. We have then added to this method another independent determination approach of n based on the work of Li et al. [12]. This approach is called the "multistep pressure" method and is described in the next section.

Multistep pressure approach for a separate identification of n

In this method, different successive steps of pressure are investigated in a classical die compaction SPS experiment and in isothermal condition. The value of n can be identified by the typical acceleration of the strain rate resulting from the pressure "jump" from one step to another [12]. If the difference of porosity between the two steps of pressure is small, the relation allowing to calculate n is given by:

$$n = \frac{\ln\left(\frac{|\dot{\varepsilon}_{z1}|}{|\dot{\varepsilon}_{z2}|}\right)}{\ln\left(\frac{\sigma_{z1}}{\sigma_{z2}}\right)} \tag{2}$$

where the indices 1 and 2 indicate the different compressive strain rates $\dot{\varepsilon}_z$ and stress isobar σ_z before and after the pressure "jump."

However, if the transition time between the two pressures is long or if the pressures difference is too high, a slight change of microstructure (mainly the porosity) can influence the n determination using Eq. (2). To account the eventual microstructure change during the pressure "jump," a more general and comprehensive form of Eq. (2) has been determined by Li et al. [12]:

$$n = \frac{\ln\left(\frac{\exp(-|\varepsilon_{z2}|)-(1-\theta_0)|\dot{\varepsilon}_{z1}|}{\exp(-|\varepsilon_{z1}|)-(1-\theta_0)|\dot{\varepsilon}_{z2}|}\right)}{\ln\left(\frac{\sigma_{z1}}{\sigma_{z2}}\exp(|\varepsilon_{z2}|-|\varepsilon_{z1}|)\sqrt{\frac{\exp(-|\varepsilon_{z2}|)-(1-\theta_0)}{\exp(-|\varepsilon_{z1}|)-(1-\theta_0)}}\right)} \tag{3}$$

with θ_0 the initial porosity.

This method is specifically dedicated to the identification of n. The other advantage of this approach is that it can be applied to the SPS in closed conditions to the first study (die compaction with graphite tools, pulsed electric current, vacuum atmosphere etc.). For the theoretical point of view, Eq. (3) has been determined with the same powder densification model used in the regression method (Olevsky [2]) and the same hypothesis of mechanical moduli φ and ψ (Skorohod [13]). The two methods are then coherent to each other as they use the same model and hypothesis. This method is investigated to calculate a value of n that can be compared to the value obtained qualitatively using the first regression method. A discussion on the accuracy the n determination with both approaches will be done for varied materials. The influence of the mechanical moduli φ and ψ on creep parameters identification will be also discussed.

Experiments

All the experiments where performed on an SPS machine (Dr. Sinter 2080, SPS Syntex Inc, Japan) of the Plateforme Nationale CNRS de Frittage Flash located at the University of Toulouse III-Paul Sabatier. Three tests were carried out for the regression method experiments; one was meant to determine the specimen displacement, another one to subtract the elastic and thermal expansion contributions and the last one to determine the sample temperature by an additional K type thermocouple placed in the powder. Six different powders of 4Y-ZrO_2 (from Tosoh) for the ceramic, Fe (from Fluka), Ti–6Al–4V (from Aubert & Duval) and Al (from Goodfellow) for the metals and alloys, poly(methyl methacrylate) (PMMA from Aldrich) and polystyrene (PS from Goodfellow) for the polymers were analyzed. These powders have been selected to represent the behavior of the three main classes of materials from polymers (PMMA, PS), low-temperature metal (Al, Fe), high temperature alloy (Ti–6Al–4V) to ceramics (4Y-ZrO_2). The multistep method has been used for all metal and ceramic samples in classical SPS die compaction configuration and isotherm conditions. The dwell temperature has been reached by a 100 K/min temperature ramp followed by the holding of 250 °C for Al, 600 °C for Fe 850 °C for Ti–6Al–4V and 1100 °C for 4Y-ZrO_2, After stabilization of the temperature, about 3–4 successive pressure steps were generated manually in order to measure the variation of strain rate at each pressure "jump." Different values of n are determined to calculate a standard deviation to estimate the error of the method. For each multistep tests, the thermal expansion can be neglected because

the experiments are in isothermal conditions, but the sample real temperature has been determined separately by an additional experiment with a thermocouple in the powder.

Results and discussion

In a first section, the outcome of the regression and multistep method for different materials is presented and discussed. The next section is a discussion on the influence of the mechanical moduli on the extracted creep parameters. In this section, the regression method is expressed using the Abouaf model and experimental moduli we previously determined for Ti–6Al–4V. This fully experimental approach enables the comparison of the creep parameters identified by experimental/theoretical moduli and reveals the accuracy of the first methodology.

Determination of the creep parameters by regression and multistep approaches

The experimental sintering curves of each of the powders studied are reported in Fig. 1. Due to the fact that all of these materials have very different sintering temperatures, different conditions have been examined for each one of these powders (*see the experimental conditions inserted in* Fig. 1). Setting aside polymers that have a typical viscous behavior, working out the n has been done via the multistep method [12] in isothermal conditions on all the other materials. The typical stress/displacement curves for all the materials tested by multistep method are reported in Fig. 2, and the n values extracted from these curves are provided in Table 1. The average n values are estimated using Eq. (3) and the strain/strain rate/stress values before and after each pressure "jump" [12]. The location of the measures of strain rate used in Eq (3) on the displacement curves is highlighted in Fig. 2 by blue and red lines (with in bleu the slope before the pressure "jump" and in red the slope after the pressure "jump"). In addition, all the A_0 and Q values obtained by linear regression using Eq. (1) for each n value tested ranging from 1 to 5 are reported in Table 2. Based on this data, the modeled curves for each material and each tested n can be obtained (Fig. 1). The comparison of the n qualitatively obtained using the experiment/modeled curves (Fig. 1) and the average n value resulting from the multistep method are reported in Table 1.

The curves reported in Fig. 1 point out the high sensitivity of the different modeled relative density curves shapes to the value of considered n. These differences can be quite high, like in the PS experiment and very low such as it has been observed in the Ti–6Al–4V experiment. The metals and alloy powders exhibit between 2 and 7% of densification in the range of the low temperatures. This phenomenon can be attributed to the plastic deformation of the metals particles. This phenomenon is typically not explained by our model which is restricted to the high temperature creep behavior. However, except for the case of aluminum and iron, this contribution is low on the other powders. The comparison of the curves (Fig. 1) concern then the main densification part of the curves; the initial part can be subject to discrepancy originated from plasticity and we showed previously [17] the final stage can also be disturbed by the grain growth.

Both methods indicate n values with a different range of accuracy, but they converge to similar n values. The use of the multistep method is particularly well suited for Ti–6Al–4V and Al where the qualitative evaluation of n is difficult (relative density curves are similar for the different tested n values). An n value close to 1 is observed for yttria-stabilized zirconia (YSZ) and the polymer powders. For the polymers or amorphous glass materials, a linear viscous behavior is classical [18]. Concerning YSZ, this result seems to indicate a dominant Coble grain boundary diffusion creep mechanism [19]. Similar n values, close to 1, are reported for this material in refs. [20, 21] and $n = 2$ in [22]. For iron and aluminum metals, the low-temperature densification is not accurate, but for the middle section of the curve, n values seem close to 2 for Fe and 4–5 for Al. As to Al, the n value is typical [23], for Fe the n value of the pure metal should be near 4 [24], but the value is closer to the iron oxide exponent closer to 1 [25]. For the iron powder, the hypothesis can be made that the lower n value is due to the creep behavior of an iron oxide shell as it is well known that transition metal particles are usually passivated by an oxide layer.

Influence of the mechanical moduli φ and ψ on the identified creep parameters

The determination of these parameters depends heavily on the porosity-dependent moduli here, φ and ψ that govern the mechanical field behavior in

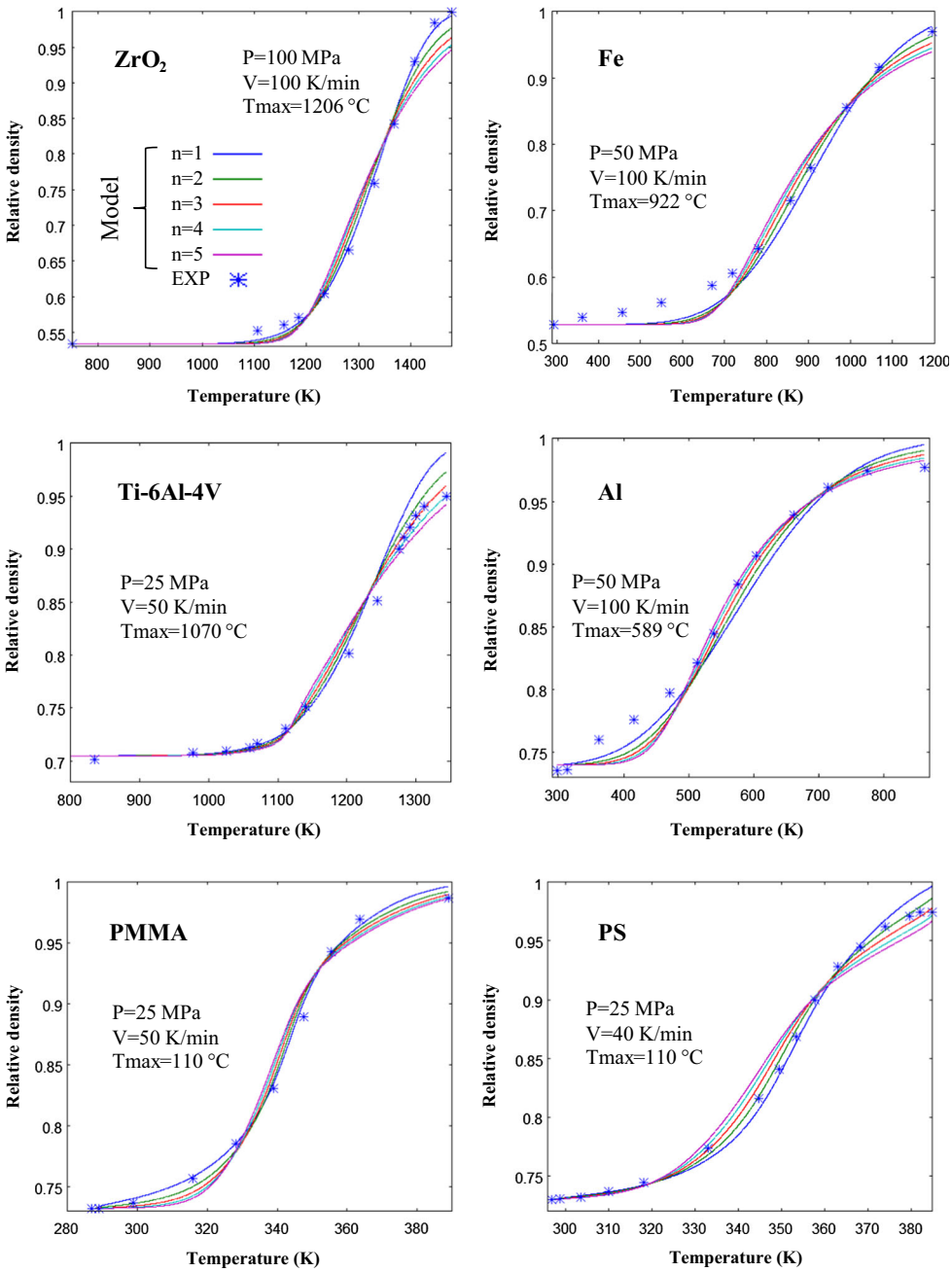

Fig. 1 Modeled/experimental relative density curves for each tested material and using the identified parameters from the regression approach.

the equivalent porous material. These parameters are generally considered using theoretical approximations such as the one we used in the regression approach (Skorohod theoretical moduli [13]). However, these moduli may evolve with the material and/or the powder morphology. Using experimentally determined moduli (instead of theoretical moduli) will thus help improve the accuracy of the identified creep coefficients preventing the compensation of these coefficients for non-adapted moduli. Such a comparison is possible on the Ti–6Al–4V case (Fig. 1) using the moduli we previously determined in ref. [8] on the same powder and using Abouaf model [7]. The regression Eq. (1) that uses the Olevsky [2] model needs then to be reformulated using the Abouaf model. Abouaf regression Eq. (4) has been determined from Eq. (5) of stress in the case of die compaction (see ref. [8]). The formulation of the regression equation using the Abouaf model is also useful because numerous experimentally determined moduli [8–10, 26–29] use this model.

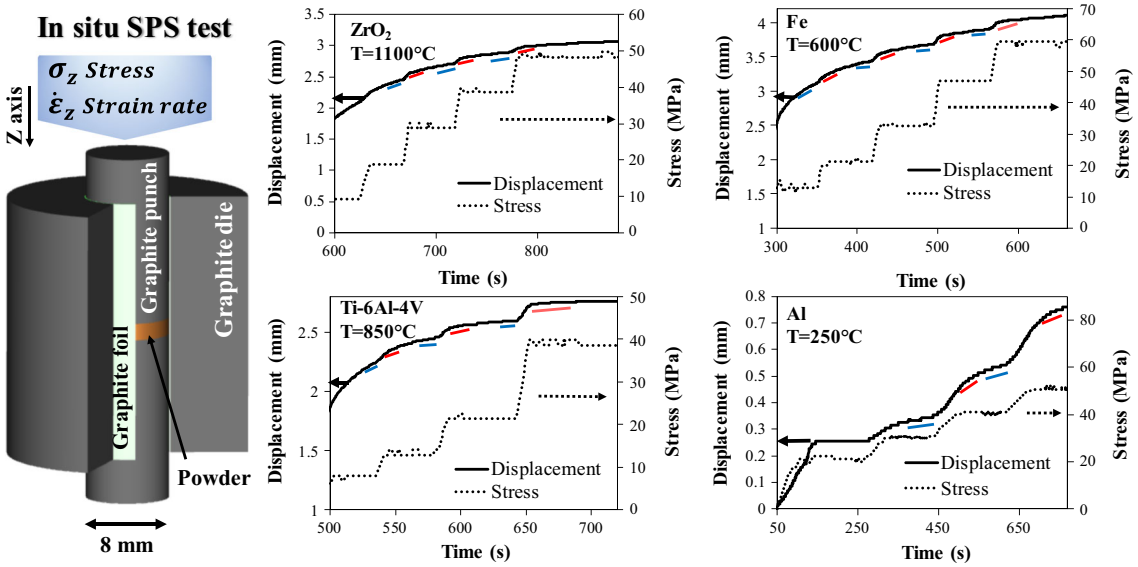

Fig. 2 Displacement and stress curves for the multistep method of Li et al.

Table 1 Comparison of the stress exponents determined independently by the multistep method (Li et al.) approach and estimated qualitatively (regression method) on the curves in Fig. 1

Materials	n multistep method	±	n qualitative
4Y-ZrO_2	1.7	0.7	1
Fe	2.2	0.4	2
TA6V	1.9	0.5	2–3
Al	5.4	0.9	4–5

$$\ln\left(\left(\frac{|\dot{\varepsilon}_z|^{\frac{1}{n}}\left(\frac{4}{c}+\frac{1}{f}\right)^{\frac{n+1}{2n}}}{9\left(\frac{1}{3}\right)^{\frac{n-1}{n}}|\sigma_z|}\right)^{n}\right)+\ln(T)=\ln(A_0)-\frac{Q}{RT} \quad (4)$$

$$|\sigma_z|=A^{-\frac{1}{n}}|\dot{\varepsilon}_z|^{\frac{1}{n}}\left(\frac{1}{3}\right)^{\frac{1-n}{n}}\left(\frac{4}{c}+\frac{1}{f}\right)^{\frac{n+1}{2n}}\frac{1}{9} \quad (5)$$

where c and f are the Abouaf shear and bulk moduli.

Equation (4) was tested on Ti–6Al–4V, and the experimental c and f moduli of Ti–6Al–4V can be found in Ref. [8]: their fitting expression is reported below.

$$f=0.023\left(\frac{(1-\rho)}{(\rho-0.67)}\right)^{1.5} \quad (6)$$

$$c=1+130\left(\frac{(1-\rho)}{(\rho-0.2)}\right)^{1.3} \quad (7)$$

where ρ is the relative density.

The complete methodology applied to the Abouaf model is reported in Fig. 3 with on the right side, the regression curves for the determination of A_0 and Q for different n values, and on the left, each modeled densification curves using the determined creep parameters. Like for the previous approach (Fig. 1 for Ti–6Al–4V), this new approach using experimentally

Table 2 Identified creep parameters using the regression method (with A_0 in K s^{-1} Pa^{-n} and Q in kJ mol^{-1})

n		4Y-ZrO_2	Al	Fe	TA6V	PMMA	PS
1	Q	221	23.2	49.0	198	52.7	62.5
	A_0	6.02E1	9.30E−6	5.66E−5	8.39E1	1.80E1	3.83E2
2	Q	288	33.8	67.5	228	76.6	75.7
	A_0	3.13E−4	3.61E−12	1.64E−11	1.00E−4	6.35E−3	3.24E−3
3	Q	356	44.3	86.0	259	101	88.9
	A_0	1.63E−9	1.40E−18	4.73E−18	1.20E−10	2.24E−6	2.74E−8
4	Q	423	54.9	104	289	124	102
	A_0	8.47E−15	5.45E−25	1.37E−24	1.44E−16	7.88E−10	2.32E−13
5	Q	491	65.5	123	319	148	115
	A_0	4.40E−20	2.12E−31	3.95E−31	1.72E−22	2.78E−13	1.97E−18

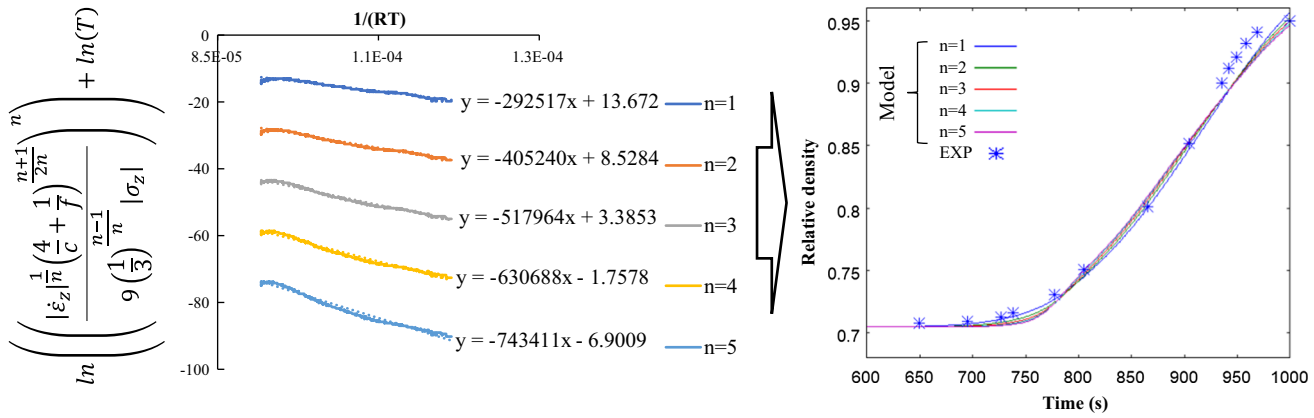

Fig. 3 Regression method applied to the Abouaf model and for Ti–6Al–4V.

determined c and f succeeds in explaining the main experimental data points. Some discrepancy can be observed at the end of the sintering stage between the experimental points and the simulated curves. Like previously, the n qualitative identification is also difficult as the variation of the modeled curves with n is particularly small in this case. The value of creep activation energy experimentally measured in Ref. [8] for $n = 2$ is 416 kJ mol^{-1} which is close to the present identified value of 405 kJ mol^{-1} but far from the 228 kJ mol^{-1} value determined using theoretical compaction moduli (see Table 2). This example clearly illustrates the compensation that occurs on the identified creep parameters to correct the curves when theoretical moduli are employed. In other words, the identified creep parameters (A_0 and Q) correct the eventual mistake originated from the difference between the experimental and theoretical moduli.

Conclusion

The capacity of the regression approach to predict spark plasma sintering densification in a wide range of materials has been analyzed, and three main conclusions are highlighted.

- Firstly, this approach of densification parameters extraction is fast and successful for the establishing of the densification model regardless of the materials. The model/experiment error is less than 7%. For the metals, 2–7% of discrepancy is associated with a phenomenon of plasticity at low temperatures not considered by the model.
- The combination of the regression method (which is very efficient to determine the creep parameters A_0 and Q) and the multistep method of Li et al. for the independent determination of n is particularly well suited for materials in which the qualitative estimation of n (by the regression approach) is difficult.
- Finally, the comparison for Ti–6Al–4V of the regression with theoretical/experimental moduli shows different identified creep parameters for a same densification curve. When theoretical moduli are employed, the identified creep parameters compensate the eventual moduli discrepancy; these creep parameters can then be considered more as equivalent parameters.

Acknowledgements

C.M. and C.E. thank the French National Research Agency (ANR) for funding this study as part of the ANR09 MAPR-007 Impulsé project.

References

[1] Olevsky EA, Garcia-Cardona C, Bradbury WL et al (2012) Fundamental aspects of spark plasma sintering: II. Finite element analysis of scalability. J Am Ceram Soc 95:2414–2422. https://doi.org/10.1111/j.1551-2916.2012.05096.x

[2] Olevsky EA (1998) Theory of sintering: from discrete to continuum. Mater Sci Eng R Rep 23:41–100. https://doi.org/10.1016/S0927-796X(98)00009-6

[3] Guillon O, Gonzalez-Julian J, Dargatz B et al (2014) Field-assisted sintering technology/spark plasma sintering: mechanisms, materials, and technology developments. Adv Eng Mater 16:830–849. https://doi.org/10.1002/adem.201300409

[4] Chaim R (2013) Electric field effects during spark plasma sintering of ceramic nanoparticles. J Mater Sci 48:502–510. https://doi.org/10.1007/s10853-012-6764-9

[5] Rybakov KI, Olevsky EA, Semenov VE (2012) The microwave ponderomotive effect on ceramic sintering. Scr Mater 66:1049–1052. https://doi.org/10.1016/j.scriptamat.2012.02.043

[6] Lee G, Olevsky EA, Manière C et al (2018) Effect of electric current on densification behavior of conductive ceramic powders consolidated by spark plasma sintering. Acta Mater 144:524–533. https://doi.org/10.1016/j.actamat.2017.11.010

[7] Abouaf M, Chenot JL, Raisson G, Bauduin P (1988) Finite element simulation of hot isostatic pressing of metal powders. Int J Numer Methods Eng 25:191–212. https://doi.org/10.1002/nme.1620250116

[8] Manière C, Kus U, Durand L et al (2016) Identification of the norton-green compaction model for the prediction of the Ti–6Al–4V densification during the spark plasma sintering process. Adv Eng Mater 18:1720–1727. https://doi.org/10.1002/adem.201600348

[9] Martins D, Grumbach F, Manière C et al (2017) In-situ creep law determination for modeling Spark Plasma Sintering of TiAl 48-2-2 powder. Intermetallics 86:147–155. https://doi.org/10.1016/j.intermet.2017.03.006

[10] Manière C, Olevsky EA (2017) Porosity dependence of powder compaction constitutive parameters: determination based on spark plasma sintering tests. Scr Mater 141:62–66. https://doi.org/10.1016/j.scriptamat.2017.07.026

[11] Manière C, Durand L, Weibel A, Estournès C (2016) Spark-plasma-sintering and finite element method: from the identification of the sintering parameters of a submicronic α - alumina powder to the development of complex shapes. Acta Mater 102:169–175. https://doi.org/10.1016/j.actamat.2015.09.003

[12] Li W, Olevsky EA, McKittrick J et al (2012) Densification mechanisms of spark plasma sintering: multi-step pressure dilatometry. J Mater Sci 47:7036–7046. https://doi.org/10.1007/s10853-012-6515-y

[13] Skorohod V (1972) Rheological basis of the theory of sintering. Nauk Dumka, Kiev, p 72–250

[14] Wang J, Raj R (1990) Estimate of the activation energies for boundary diffusion from rate-controlled sintering of pure alumina, and alumina doped with zirconia or titania. J Am Ceram Soc 73:1172–1175. https://doi.org/10.1111/j.1151-2916.1990.tb05175.x

[15] Rahaman MN (2007) Sintering of ceramics. CRC Press, Boca Raton, p 1–100

[16] Manière C, Durand L, Estournès C (2016) Powder/die friction in the spark plasma sintering process: modelling and experimental identification. Scr Mater 116:139–142. https://doi.org/10.1016/j.scriptamat.2016.01.040

[17] Manière C, Durand L, Weibel A, Estournès C (2016) A predictive model to reflect the final stage of spark plasma sintering of submicronic α-alumina. Ceram Int 42:9274–9277. https://doi.org/10.1016/j.ceramint.2016.02.048

[18] German RM (1996) Sintering theory and practice. Wiley, New York, p 80–82

[19] Coble RL (1963) A model for boundary diffusion controlled creep in polycrystalline materials. J Appl Phys 34:1679–1682. https://doi.org/10.1063/1.1702656

[20] Seltzer MS, Talty PK (1975) High-temperature creep of Y_2O_3-stabilized ZrO_2. J Am Ceram Soc 58:124–130. https://doi.org/10.1111/j.1151-2916.1975.tb19574.x

[21] Dimos D, Kohlstedt DL (1987) Diffusional creep and kinetic demixing in yttria-stabilized zirconia. J Am Ceram Soc 70:531–536. https://doi.org/10.1111/j.1151-2916.1987.tb05700.x

[22] Bernard-Granger G, Guizard C (2007) Spark plasma sintering of a commercially available granulated zirconia powder: I. Sintering path and hypotheses about the mechanism(s) controlling densification. Acta Mater 55:3493–3504. https://doi.org/10.1016/j.actamat.2007.01.048

[23] Ma ZY, Tjong SC (1999) The high-temperature creep behaviour of 2124 aluminium alloys with and without particulate and SiC-whisker reinforcement. Compos Sci Technol 59:737–747. https://doi.org/10.1016/S0266-3538(98)00113-4

[24] Shi L, Wang Z-G, Zhang S-L (2015) Creep deformation of ductile cast iron cooling staves. Ironmak Steelmak 42:339–345. https://doi.org/10.1179/1743281214Y.0000000234

[25] Crouch AG (1972) High-temperature deformation of polycrystalline Fe_2O_3. J Am Ceram Soc 55:558–563. https://doi.org/10.1111/j.1151-2916.1972.tb13436.x

[26] Nicolle C (1999) Mise en forme de poudre de bore par compression isostatique à chaud: determination des propriétés rhéologiques et simulation numérique du procédé. Université de Bourgogne, France

[27] Besson J (1990) Simulation numerique de la mise en forme des ceramiques application a la compaction isostatique a chaud. L'ecole nationale superieure des mines de Paris

[28] Geindreau C, Bouvard D, Doremus P (1999) Constitutive behaviour of metal powder during hot forming.: Part II: unified viscoplastic modelling. Eur J Mech A Solids 18:597–615. https://doi.org/10.1016/S0997-7538(99)00101-1

[29] Wolff C, Mercier S, Couque H et al (2016) Thermal-electrical-mechanical simulation of the nickel densification by Spark Plasma Sintering. Comparison with experiments. Mech Mater 100:126–147. https://doi.org/10.1016/j.mechmat.2016.06.012